Check for updates

View Article Online
View Journal

PCCP

Accepted Manuscript

This article can be cited before page numbers have been issued, to do this please use: D. Liang, J. Hong, F. Dong, J. Bennett, S. E. Mason, R. Hamers and Q. Cui, *Phys. Chem. Chem. Phys.*, 2017, DOI: 10.1039/C7CP06709G.

This is an Accepted Manuscript, which has been through the Royal Society of Chemistry peer review process and has been accepted for publication.

Accepted Manuscripts are published online shortly after acceptance, before technical editing, formatting and proof reading. Using this free service, authors can make their results available to the community, in citable form, before we publish the edited article. We will replace this Accepted Manuscript with the edited and formatted Advance Article as soon as it is available.

You can find more information about Accepted Manuscripts in the author guidelines.

Please note that technical editing may introduce minor changes to the text and/or graphics, which may alter content. The journal's standard Terms & Conditions and the ethical guidelines, outlined in our author and reviewer resource centre, still apply. In no event shall the Royal Society of Chemistry be held responsible for any errors or omissions in this Accepted Manuscript or any consequences arising from the use of any information it contains.

ROYAL SOCIETY OF CHEMISTRY

rsc.li/pccp

View Article Online
DOI: 10.1039/C7CP06709G

Published on 30 November 2017. Downloaded by University of Wisconsin - Madison on 30/11/2017 14:59:34.

Physical Chemistry Chemical Physics Accepted Manuscript

Analysis of Conformational Properties of Amine Ligands at the Gold/Water Interface with QM, MM and QM/MM simulations

Dongyue Liang,[†] Jiewei Hong,[†] Dong Fang,[†] Joseph W. Bennett,[‡] Sara E. Mason,[‡] Robert J. Hamers,[¶] and Qiang Cui*,[†]

†*Department of Chemistry and Theoretical Chemistry Institute, University of Wisconsin-Madison, 1101 University Avenue, Madison, WI 53706*

‡*Department of Chemistry, University of Iowa, 251 North Capitol Street, Iowa City, IA 52242*

¶*Department of Chemistry, University of Wisconsin-Madison, 1101 University Avenue, Madison, WI 53706*

E-mail: cui@chem.wisc.edu, Tel:(+1)-608-332-6584

Abstract

We describe a strategy of integrating quantum mechanical (QM), hybrid quantum mechanical/molecular mechanical (QM/MM) and MM simulations to analyze physical properties of solid/water interface. The protocol involves using a correlated *ab initio* (CCSD(T)) method to first calibrate Density Functional Theory (DFT) as the QM approach, which is then used in QM/MM simulations to compute relevant free energy quantities at the solid/water interface using a mean-field approximation of Yang et al. that decouples QM and MM thermal fluctuations; gas-phase QM/MM and periodic DFT calculations are used to determine the proper QM size in the QM/MM

View Article Online
DOI: 10.1039/C7CP06709G

Published on 30 November 2017. Downloaded by University of Wisconsin - Madison on 30/11/2017 14:59:34.

simulations. Finally, QM/MM free energy results are compared with those from MM simulations to directly calibrate the force field model for the solid/water interface. The protocol is illustrated by examining the orientations of an alkyl amine ligand at the gold/water interface, since the ligand conformation is expected to impact the chemical properties (e.g., charge) of the solid surface. DFT/MM and MM simulations using the INTERFACE force field lead to consistent results, suggesting that the effective gold/ligand interaction can be adequately described by a van der Waals model, while electrostatic and induction effects are largely quenched by solvation. The observed differences among periodic DFT, QM/MM and MM simulations, nevertheless, suggest that explicitly including electronic polarization and potentially charge transfer in the MM model can be important to the quantitative accuracy. The strategy of integrating multiple computational methods to cross-validate each other for complex interfaces is applicable to many problems that involve both inorganic/metallic and organic/biomolecular components, such as functionalized nanoparticles.

Physical Chemistry Chemical Physics Accepted Manuscript

View Article Online
DOI: 10.1039/C7CP06709G

Published on 30 November 2017. Downloaded by University of Wisconsin - Madison on 30/11/2017 14:59:34.

Physical Chemistry Chemical Physics Accepted Manuscript

1 Introduction

Nanoparticles are playing increasingly important roles in many technological applications such as imaging, drug delivery, energy conversion and catalysis. To ensure that nanotechnology is sustainable, it is important to understand how nanoparticles interact with environment and biological systems as well as the physicochemical principles that dictate such interactions.[1,2] Since nanoparticles are often decorated with ligands for function and stability considerations, a necessary task is to determine the properties of these surface ligands, which likely control how nanoparticles interact with other (bio)molecules. For example, it has been well established that the charge state of nanoparticle ligands has a major impact on the binding affinity of nanoparticles to lipid membranes;[3] *in vivo* studies also showed that the toxicity of nanoparticles to *Daphnia magna* depends critically on the charge of nanoparticles, and that cationic ligands appear to lead to a higher level of toxicity.[4]

Experimentally, the charge of nanoparticles is often inferred from the measurement of ζ-potential, which is not straightforward to interpret at the microscopic level. Therefore, several research groups developed computational approaches for the determination of pK_a of surface ligands and thus the charge state of nanoparticles.[5,6] For these computational approaches to be predictive, it is essential to properly describe the conformational distribution of ligands at the nanoparticle/water interface, since the environment (e.g., the degree of hydration) for the titratable groups is expected to be a critical factor that determines the pK_a and apparent charge of ligands;[6] conformational flexibility of the surface ligands may also influence the interfacial solvent fluctuations, which in turn determines the hydrophobic/hydrophilic nature of the interface.[7] To sample the conformational distribution of surface ligands at ambient condition, molecular simulations using classical force fields are required; an important component of the investigation, therefore, is to validate the force field model for the description of ligand conformational properties at the nanoparticle/water interface. For this purpose, experimental data at the relevant spatial resolution is scarcely available, thus it is valuable to establish an effective calibration protocol using computations. This is

View Article Online
DOI: 10.1039/C7CP06709G

Published on 30 November 2017. Downloaded by University of Wisconsin - Madison on 30/11/2017 14:59:34.

Physical Chemistry Chemical Physics Accepted Manuscript

not a trivial matter as no single computational method is sufficient for a quantitative analysis of solid/liquid interfaces. In this work, using amine ligands at the gold/water interface as an example, we show that combining results from full quantum mechanical (QM) calculations, hybrid quantum mechanical/molecular mechanical (QM/MM) and pure MM simulations provides a comprehensive analysis of the reliability and consistency of computational models for ligands at an interface; while our work is motivated by the ultimate goal of analyzing properties of nanoparticles, we chose the simpler model system that involves a slab model for the solid, which is sufficient for comparing different computational methodologies. We encourage this type of analysis as a critical validation step for the study of other solid/liquid interfaces.

In the following, we first summarize the computational methodologies used in this work; in particular, we discuss the use of a minimum free energy QM/MM approach to bridge the comparison between pure MM simulation and full QM based calculations. We then present results for the conformational properties of amine ligands at the gold/water interface using multiple computational methods and analyze the level of consistency among the results. Finally, we draw a few conclusions.

2 Computational Models and Methods

The specific model system under study here is an alkyl amine on the (111) surface of a gold surface immersed in water; the alkyl amine is covalently attached to the gold surface through a gold-thiol bond. The amine ligand is chosen here because it is often used to functionalize nanoparticles and its titration behavior on the surface of a nanoparticle has been analyzed in our recent work.[6] As discussed in detail below, two orientations of the alkyl amine (see Fig. 1) have been identified, which are referred to as the "parallel" and "vertical" orientations in the subsequent discussions. The relative stability of the two orientations is the quantity of primary interest in this work, since the relative population is expected to have an impact

View Article Online
DOI: 10.1039/C7CP06709G

Published on 30 November 2017. Downloaded by University of Wisconsin - Madison on 30/11/2017 14:59:34.

on the pK_a of the amine group, which will be analyzed in separate work. For comparison, MM simulations have also been conducted for the same alkyl amine ligand (without the thiol group) covalently attached to the (111) surface of hydrogen-terminated diamond.

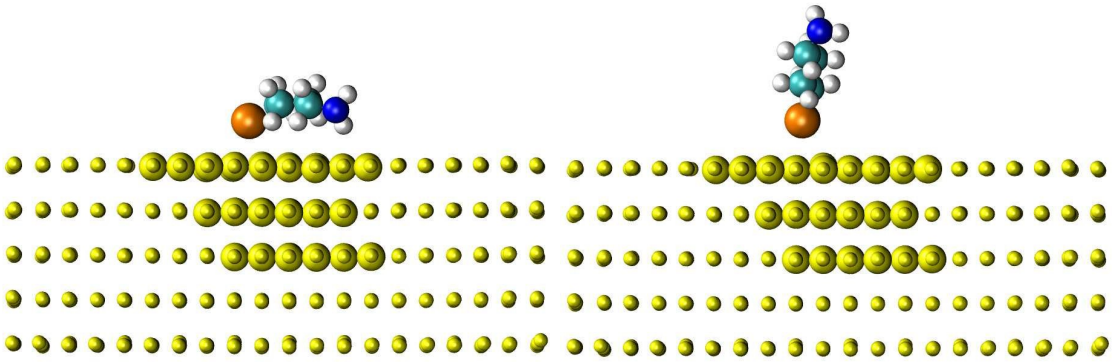

(a) (b)

Figure 1: Illustration for the (a) parallel and (b) vertical orientations of an alkyl amine covalently attached to the (111) surface of gold through a gold-thiol bond. Both protonated and deprotonated states of the amine have been studied. Atoms treated as QM in the solution QM/MM simulations are highlighted as larger spheres (color representations: yellow - Au, orange - S, green - C, blue - N, white - H); for clarity, water molecules and salt ions are not shown.

It's worth emphasizing why it is important to examine multiple computational methods for the validation and calibration of force field models for solid/liquid interfaces. Since most empirical force fields use highly simplified functional forms, they are effective models developed for condensed phase simulations; therefore, it is usually not appropriate to directly compare results of popular (bio)molecular force fields (e.g., CHARMM[8,9] and AMBER[10] for biomolecules and INTERFACE,[11] which has been developed in a similar framework as CHARMM) to QM calculations for gas phase systems. For condensed phase systems or interfaces, however, full QM calculations are computationally prohibitive for achieving statistical convergence. Our strategy, therefore, is to compare relevant free energy quantities from MM and QM(DFT)/MM simulations; the free energy from MM is computed using umbrella sampling, while DFT/MM free energy is computed using a mean-field approach introduced by Yang and co-workers for biomolecular applications[12] (see discussion below).

Physical Chemistry Chemical Physics Accepted Manuscript

View Article Online
DOI: 10.1039/C7CP06709G

Published on 30 November 2017. Downloaded by University of Wisconsin - Madison on 30/11/2017 14:59:34.

Physical Chemistry Chemical Physics Accepted Manuscript

To further calibrate the DFT/MM methodology, we conduct full QM (DFT and CCSD(T)) calculations for cluster models in the gas phase and DFT calculations for a periodic slab model; the cluster model calibrates DFT against *ab initio* QM methods, and comparison of the cluster and slab models tests the validity of treating a small region ($\sim$ 50 atoms) as QM in QM/MM calculations for the gold/water interface.

Below we first summarize the details for the MM simulations, then the full QM calculations for the cluster and slab models; finally, we discuss QM/MM calculations in the gas phase and solution.

2.1 MM simulations

MM simulations for the gold/water interface have been conducted using the INTERFACE force field;[11] the specific version of the force field adopted here is non-polarizable and treats each gold atom as a charge-neutral Lennard-Jones particle. Despite simplicity, the model has been shown to provide an adequate description of the structural features of bulk gold and several interfaces.[13] Whether explicit electronic polarization, which has been shown to be important to the binding of charged molecules at metal/water interface[14] but not explicitly included here, has a major impact on the relative stability of the two ligand orientations is one of the questions we seek to answer in this study. The water molecules are treated with the TIP3P model,[15] and the ligand is described with parameters of similar amino acid sidechains in the CHARMM force field for proteins;[8,9] both protonated and deprotonated states of the amine have been studied. For comparison, the same alkyl amine ligand (without the thiol linkage) is studied on a hydrogen terminated (111) surface of diamond immersed in water. The diamond is described by atom type CT1 (aliphatic sp^3 C for CH) in the CHARMM36 protein force field.

Two types of simulations are carried out for each interface. First, unrestrained MD simulations are conducted with multiple ligands on the surface; two ligand densities, which represent high ($\sim$10 molecules/nm^2) and moderate ($\sim$2-3 molecules/nm^2) density cases, are

View Article Online
DOI: 10.1039/C7CP06709G

Published on 30 November 2017. Downloaded by University of Wisconsin - Madison on 30/11/2017 14:59:34.

Physical Chemistry Chemical Physics Accepted Manuscript

studied for both gold and diamond surfaces; in a recent experimental study,[4] for example, the ligand density was measured[16] to be $\sim$ 4-5 molecule/nm^2. Each system consists of a five-layer diamond/gold slab with a surface area of 3.0×3.0 nm^2. The slab, whose structure is held fixed, is then immersed in a cubic water box with a length of 5 nm, which also contains 0.15 M of KCl (the impact of salt is, however, minor, as shown in Fig. S1 in **Supporting Information**). Electrostatic interactions are treated with Particle-Mesh-Ewald[17] with a grid $\sim$ 1 Å and a real-space cutoff of 1.2 nm. Van der Waals interactions are treated with the switch scheme[18] for distance between 1.0 and 1.2 nm. Simulations are conducted with an NVT ensemble at 300 K using Langevin dynamics and a damping coefficient of 1.0 ps^{-1}. All bonds involving hydrogen are constrained using RATTLE.[19] The system is equilibrated for 2 ns, which is followed by a production run of 30 ns with a time-step of 2 fs.

To further explore the intrinsic conformational preference of the ligand, umbrella sampling simulations are conducted for a single alkyl amine at the interface; the potential of mean force (PMF) is computed along the reaction coordinate $d_{N,\text{surface}}$, which is the distance between the ligand nitrogen and the surface. For each system, 40 windows are used for umbrella sampling, for which the centers of the umbrella potential are evenly distributed from 2.45 to 10.25 Å for $d_{N,\text{surface}}$. The force constant is 15.0 $kcal/(mol \cdot \mathring{A}^2)$ for all windows. PMF is computed from the umbrella sampling data using WHAM[20] with 200 bins; the convergence tolerance is set to be 10^{-6} kcal/mol.

2.2 Full QM calculations

2.2.1 Cluster calculations

To help calibrate the QM method in QM/MM simulations, we study several cluster models. As shown in Fig. 2, two small gold clusters are used to probe their interactions with the amine ligand through covalent and non-covalent interactions; the small size of these models makes it possible to compare various DFT methods with CCSD(T) calculations. We mainly test two popular functionals, PBE[21,22] and B3LYP,[23–26] with or without Grimme's D3 (GD3)

View Article Online
DOI: 10.1039/C7CP06709G

Published on 30 November 2017. Downloaded by University of Wisconsin - Madison on 30/11/2017 14:59:34.

Physical Chemistry Chemical Physics Accepted Manuscript

empirical dispersion,[27] although several other functionals have also been tested (see Table 1 below); previous benchmark studies[28,29] that focused on smaller Au-ligand systems found that PBE-GD3 and TPSSh are among the best functionals compared to CCSD(T) calculations. The basis set is cc-pVTZ for non-metallic atoms (C, N, H and S)[30] and cc-pVTZ basis set with effective core potential for gold;[31] the g function was excluded on Au to reduce computational cost, and test calculations indicate that the impact on the binding energies of interest is modest and smaller than 1 kcal/mol. Smaller basis sets (Lanl2DZ[32] for Au and 6-31G(d)[33,34] for other elements) are also tested (results summarized in the **Supporting Information**) since they are used for QM/MM calculations. The structures are first optimized using PBE without the D3 dispersion correction, then a series of single point energy computations with different Au-ligand distances (labeled as d in Fig. 2) are performed with the ligand/cluster internal structure held fixed[1]; the same set of structures is used for energy calculations at different levels of QM methods. All CCSD(T) and DFT calculations are performed using the Gaussian09 package.[35]

2.2.2 Periodic DFT calculations

To further test the effect of the QM region size on the ligand orientation, we conduct periodic DFT calculations for a single alkyl amine on a (111) gold surface. Spin-polarized periodic DFT geometry optimization calculations are performed using the DMol^3 package developed by Delley,[36,37] and carried out with the PBE functional.[21,22] All geometry optimizations are converged to at least 1×10^{-3} eV/Å, and a DNP numerical atom-centered basis set is used to expand the single electron orbitals of the effective core pseudopotentials with a cutoff radius of 4.5 Å. A Monkhorst-Pack (MP) k-point grid[38] of $2 \times 2 \times 1$ is used to sample the Brillouin zone (and a thermal smear of 0.02 hartree is used).

The substrate is a 2×2 cell doubled Au (111) surface that contains 144 total Au atoms in

[1]Structures for the deprotonated amine interacting with the gold cluster (Fig. 2c) are obtained by simply removing one proton from the structures for the protonated amine (Fig. 2d); this is because optimization for the deprotonated amine leads to N-H bond activation by the gold cluster.

View Article Online
DOI: 10.1039/C7CP06709G

Published on 30 November 2017. Downloaded by University of Wisconsin - Madison on 30/11/2017 14:59:34.

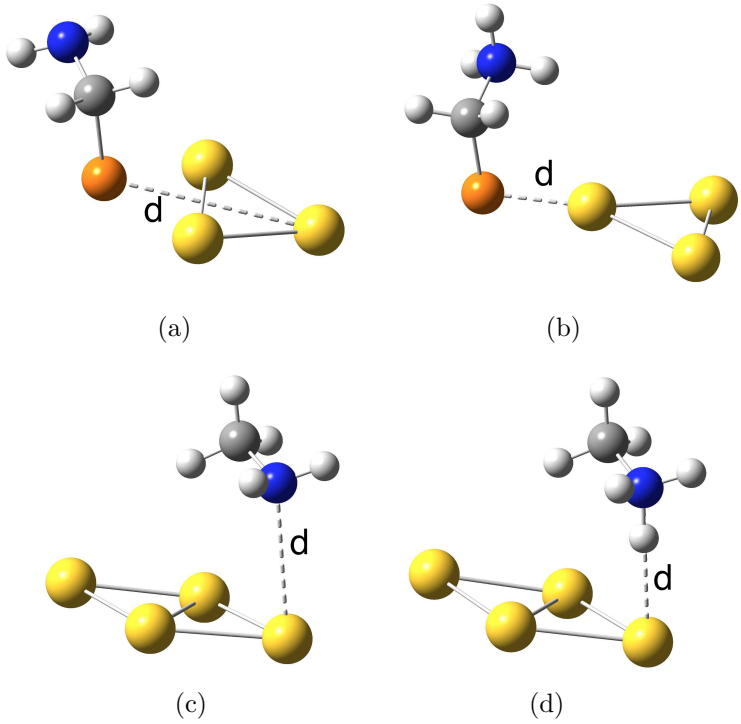

Figure 2: Illustration of model systems for calibrating bonding interaction [(a) and (b)] and adsorption [(c) and (d)] of alkyl amines to gold. The dash lines represent the reaction coordinate d defined in potential energy scans (see Fig. 7). (Color representations: yellow - Au, orange - S, gray - C, blue - N, white - H).

Physical Chemistry Chemical Physics Accepted Manuscript

View Article Online
DOI: 10.1039/C7CP06709G

Published on 30 November 2017. Downloaded by University of Wisconsin - Madison on 30/11/2017 14:59:34.

4 atomic layers. The surface and adsorbates are let to fully relax, and in all cases, the parallel configuration is preferred. Therefore, to obtain energy differences between the parallel and vertical configurations, the relaxed ligand is fixed to either configuration using gas-phase QM/MM optimized distances (see below).

2.3 QM/MM simulations

For the gold slab with a single amine ligand, QM/MM simulations are conducted for comparison.

2.3.1 Gas phase QM/MM energy optimizations

First, to determine the appropriate QM region in QM/MM simulations, we conduct gas-phase QM/MM calculations with different layers of gold atoms treated as QM (see Fig. 3); the numbers of gold atoms are chosen such that the systems are closed-shell. The structures are fully optimized (including the MM region); the QM atoms are described with the PBE-GD3 functional (Lanl2DZ basis for Au and 6-31G(d) for the rest), and the MM gold atoms are treated with the INTERFACE force field. The property of interest is the relative energy of the parallel and vertical ligand orientations.

2.3.2 Solution phase QM/MM-PMF free energy calculations

To directly compare MM simulations for the relative stability of the parallel and vertical ligand orientations, we use a mean-field type of DFT/MM simulation pioneered by Yang and co-workers for biological applications.[12] In this approach, the key quantity is the PMF for the QM atoms,

$$A(\mathbf{r}_{QM}) = -\beta^{-1} ln[\int exp(-\beta E(\mathbf{r}_{QM}, \mathbf{r}_{MM}))d\mathbf{r}_{MM}], \quad (1)$$

Physical Chemistry Chemical Physics Accepted Manuscript

View Article Online
DOI: 10.1039/C7CP06709G

Published on 30 November 2017. Downloaded by University of Wisconsin - Madison on 30/11/2017 14:59:34.

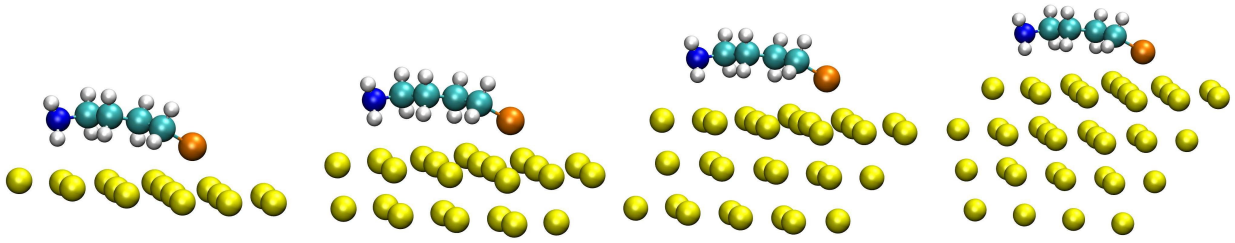

(a) (b) (c) (d)

Figure 3: Gas phase QM/MM calculations to investigate how the number of QM gold atoms influences the relative energy of the parallel and vertical ligand orientations at the surface; the results help determine the appropriate QM region in QM/MM simulations. For clarity, only the QM region is shown; the MM gold atoms are treated with the INTERFACE force field. (a), (b), (c) and (d) correspond to "single-layer", "double-layer", "triple-layer" and "quadruple-layer" models, respectively. Both protonated and deprotonated states of the amine are studied; the deprotonated cases are shown. (Color representations: yellow - Au, orange - S, green - C, blue - N, white - H)

where $E(\mathbf{r}_{QM}, \mathbf{r}_{MM})$ is the QM/MM potential energy. Geometry optimization is then conducted on the QM-PMF surface using its gradient,

$$\frac{\partial A(\mathbf{r}_{QM})}{\partial \mathbf{r}_{QM}} = \left\langle \frac{\partial E(\mathbf{r}_{QM}, \mathbf{r}_{MM})}{\partial \mathbf{r}_{QM}} \right\rangle_{\mathbf{r}_{MM}}, \tag{2}$$

where $\langle \cdots \rangle_{\mathbf{r}_{MM}}$ indicates the ensemble average over the MM degrees of freedom. To compute such ensemble average, the QM geometry is held fixed, while MM atoms are sampled using molecular dynamics (MD) at the desired temperature. During the MD simulations, the QM/MM potential energy is approximately decomposed in the following fashion ,

$$E(\mathbf{r}_{QM}, \mathbf{r}_{MM}) \approx E_{QM}(\mathbf{r}_{QM}) + E^{vdW}_{QM-MM}(\mathbf{r}_{QM}, \mathbf{r}_{MM}) + E^{elec}_{QM-MM}(\mathbf{r}_{QM}, \mathbf{r}_{MM}) + E_{MM}(\mathbf{r}_{MM}) \tag{3}$$

where $E^{vdW,elec}_{QM-MM}$ is the van der Waals/electrostatic contribution to the interaction between QM and MM atoms, and E_{QM} is the internal energy of QM atoms assumed to be independent of the MM configuration. In this work, E_{QM} is computed using a mean-field approximation, and E^{elec}_{QM-MM} is approximated with the classical Coulombic interaction between MM partial

Physical Chemistry Chemical Physics Accepted Manuscript

View Article Online
DOI: 10.1039/C7CP06709G

Published on 30 November 2017. Downloaded by University of Wisconsin - Madison on 30/11/2017 14:59:34.

charges and ESP charges for the QM atoms; different choices of ESP charges[39,40] have been tested and discussed briefly in the **Supporting Information** (Fig. S4, Table S5). $E^{vdW}_{QM-MM}(\mathbf{r}_{QM}, \mathbf{r}_{MM})$ and $E_{MM}(\mathbf{r}_{MM})$ are evaluated with the standard MM force field. Our recent analysis[41] using simple solution reactions suggested that the decomposition in Eq. 3 leads to a satisfactory approximation to the true QM/MM potential function and its gradient, although the lack of fully consistent electronic polarization in the mean-field approximation leads to errors on the order of 1 kcal/(mol·Å) in the PMF gradient. To further enhance the convergence of geometry optimization on the QM-PMF surface, an iterative scheme using fixed MM ensembles and reference QM structure is adopted; for details, see the original work of Yang and co-workers.[12]

The QM/MM-PMF calculations are conducted using an implementation into the simulation package CHARMM[42] that takes advantage of the efficient geometry optimization for the QM region using Gaussian09. The system contains 580 gold atoms (31 treated as QM), a single alkyl amine ligand (treated as QM) covalently attached to the gold surface through a thiol-gold bond, and 5,944 water molecules in the form of a droplet of 35 Å radius. A solvent boundary potential[43] in the form of a quartic potential is applied to the water molecules near the water/vacuum interface. Same as the gas phase QM/MM calculations, the QM region (see discussion in Sect.3.3) is treated with the PBE-GD3 functional and the 6-31G(d) basis for the main group elements; gold is described with the Lanl2DZ pseudo-potential and the associated basis set.[32] The MM region is described with the same force field parameters as in the MM simulations discussed above; i.e., INTERFACE for gold and TIP3P for water.

Once the geometries for the parallel and vertical orientations are optimized using the QM/MM-PMF, the relative free energy of the two orientations is computed using free energy perturbation (FEP).[44] In the FEP calculations, 23 windows are used to linearly interpolate the coordinates and ESP charges of the QM atoms between the optimized parallel and vertical structures, and the MM degrees of freedom are canonically sampled in each window (20 ps equilibration + 100 ps production). The classical free energy results are augmented

Physical Chemistry Chemical Physics Accepted Manuscript

View Article Online
DOI: 10.1039/C7CP06709G

Published on 30 November 2017. Downloaded by University of Wisconsin - Madison on 30/11/2017 14:59:34.

with contributions from the internal energy for the QM region (E_{QM} in Eq. 3), which is estimated by subtracting the interaction between QM ESP charges and MM charges from the QM/MM electrostatic energy.[41]

3 Results and Discussions

3.1 MM simulations

3.1.1 Multiple ligand simulations

The preferred ligand orientation is observed to depend on both the surface and the ligand density; the impact of protonation state of the amine is relatively minor (see discussions below), and we focus on the deprotonated case in this subsection. At the high ligand density ($\sim$10 molecules/nm^2), the ligands are expected to prefer the vertical orientation due to steric repulsions. Indeed, at the diamond surface, the amine nitrogen-surface distance ($d_{N,\text{surface}}$) distribution (Fig. 4) features two sharp peaks at large distances of $\sim$6.7 and $\sim$7.5 Å, respectively, which correspond to vertical orientations at the surface; the peak at larger $d_{N,\text{surface}}$ is due to ligands in the very center of the surface, since they experience a higher degree of steric repulsion from neighboring ligands and therefore adopt a more upright orientation compared to those near the peripheral ligands (also see discussions below in Sect.3.1.2). On the gold surface, the distribution is also bimodal but shifted toward notably smaller distances and is much broader; the distribution reaches as small distances as $\sim$4 Å, which corresponds to an almost parallel orientation.

At the moderate ligand density of 2-3 molecules/nm^2, the ligands on the diamond surface remain largely vertical, as reflected by the $d_{N,\text{surface}}$ distribution (also see Fig. 5a-b for a snapshot); the multi-modal feature remains, although the peaks are shifted towards smaller distances by $\sim$5 Å compared to the high density case. This trend is consistent with the expectation that, at the lower ligand density, the surface ligands are able to sample broader

Physical Chemistry Chemical Physics Accepted Manuscript

View Article Online
DOI: 10.1039/C7CP06709G

Published on 30 November 2017. Downloaded by University of Wisconsin - Madison on 30/11/2017 14:59:34.

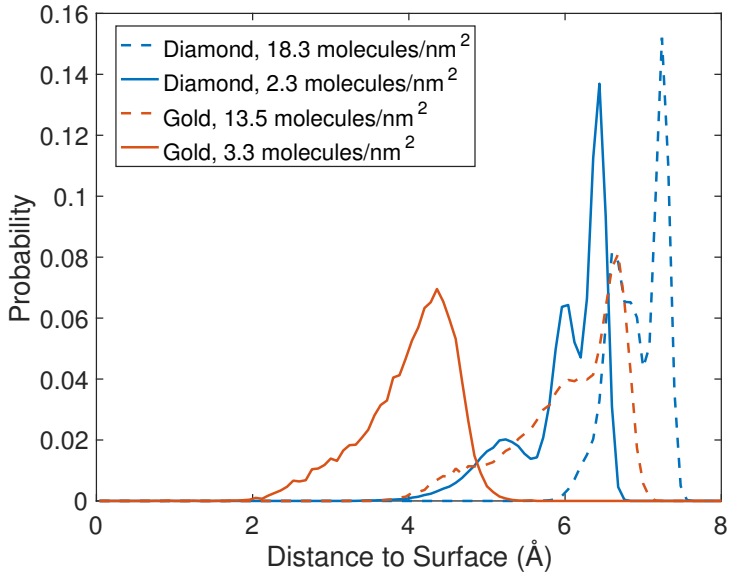

(a)

Figure 4: The distribution of ligand nitrogen - surface distances ($d_{N,\text{surface}}$) from MD simulations of functionalized (111) diamond/gold surfaces immersed in water. For clarity, only results for the deprotonated amine case is shown. Note that since the alkyl amine on the diamond surface does not have the thiol linker, to facilitate a fair comparison between the two surfaces, the $d_{N,\text{surface}}$ value for the gold case is measured relative to the plane formed by the sulfur atoms of the ligands; in all subsequent presentations for the single-ligand simulations (Fig. 6 and Table 4), $d_{N,\text{surface}}$ is defined relative to the gold surface.

Physical Chemistry Chemical Physics Accepted Manuscript

View Article Online
DOI: 10.1039/C7CP06709G

Published on 30 November 2017. Downloaded by University of Wisconsin - Madison on 30/11/2017 14:59:34.

ranges of orientations as driven by conformational entropy,[45] leading to the shift of $d_{N,\text{surface}}$ distribution towards smaller values. At the gold surface, the shift in the distribution is even more dramatic; the distribution becomes unimodal and peaks around a distance slightly larger than 4 Å. As shown by the snapshot in Fig. 5c-d, many surface ligands strongly prefer a parallel orientation to remain close to the gold surface. In a recent experimental study,[4] the ligand density for the prepared gold nanoparticle was measured to be ∼4-5 molecule/nm^2; at such a low density, results from current simulation suggest that a majority of the ligands would adopt the parallel orientation at the gold/water interface, in stark contrast to a functionalized nanodiamond surface. This difference in orientation is expected to have a substantial impact on the chemical properties of these ligands, such as pK_a and reactivity. Therefore, we conduct further analysis on the intrinsic orientational preference of a single alkyl amine ligand on the gold surface with additional quantitative calculations as discussed below.

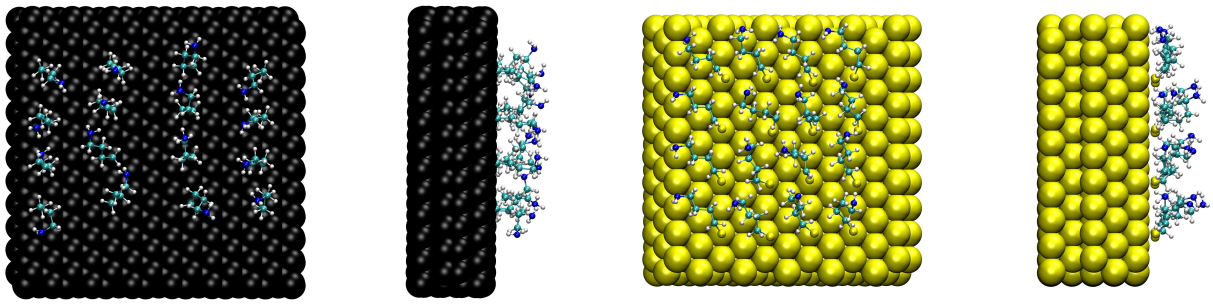

(a) (b) (c) (d)

Figure 5: Snapshots from MD simulations (top and side views) for functionalized (a-b) (111) diamond surface and (c-d) (111) gold surface immersed in water with a moderate ligand density of 2-3 mol/nm^2; water and hydrogen termination for the diamond surface are not shown for clarity; the amines are protonated. The snapshots show clear difference in ligand orientations at different surfaces (Color representations: yellow - Au, green - C, blue - N, white - H).

Physical Chemistry Chemical Physics Accepted Manuscript

View Article Online
DOI: 10.1039/C7CP06709G

Published on 30 November 2017. Downloaded by University of Wisconsin - Madison on 30/11/2017 14:59:34.

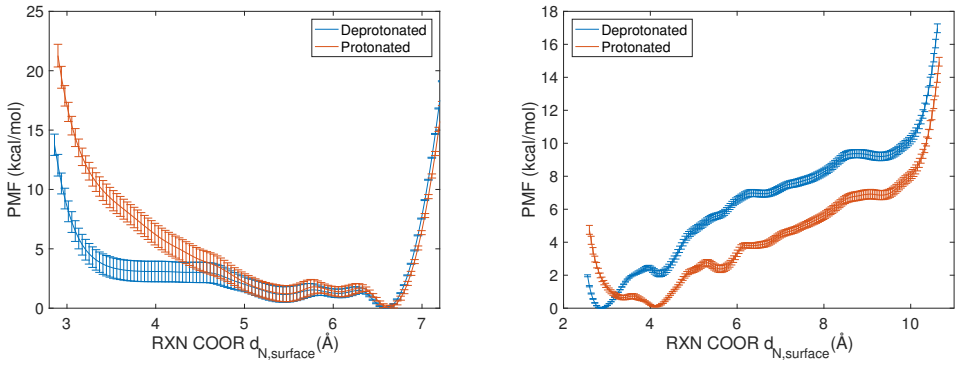

(a) (b)

Figure 6: Potential of mean force for a single alkyl amine ligand (both protonated and deprotonated states are studied) at the (a) diamond/water and (b) gold/water interface. The (111) surface is studied in both cases, and the distance from the amine nitrogen atom to the surface ($d_{N,\text{surface}}$ is chosen as the reaction coordinate).

3.1.2 Classical Potential of Mean Force (PMF) for a single ligand at the surface

The PMF results further corroborate the qualitative findings from the unbiased multiple-ligand MD simulations discussed above. At the diamond surface, regardless of the amine protonation state, the PMF (Fig. 6a) has a well at a large amine N-surface distance of 6.7 Å, which corresponds to a vertical orientation that maintains a fair amount of rotational entropy.[45] The position of the well also corresponds to the locations of the major peak in $d_{N,\text{surface}}$ distribution (Fig. 4) at moderate ligand density and of the secondary peak at high ligand density; this confirms that the primary peak in the $d_{N,\text{surface}}$ distribution observed at high ligand density reflects the steric repulsion among surface ligands that limits those in the center to adopt very upright orientations. The PMFs for the protonated and deprotonated amines are largely identical except at short $d_{N,\text{surface}}$ values; the protonated PMF goes up more quickly than the deprotonated case, likely due to the larger desolvation penalty for a protonate ligand as it approaches the surface.

At the gold/water interface, the PMFs (Fig. 6b) are qualitatively different from those at the diamond/water interface. Regardless of the amine protonation state, the PMF has a well at a short $d_{N,\text{surface}}$ value and increases rapidly at large $d_{N,\text{surface}}$ values. This trend is

Physical Chemistry Chemical Physics Accepted Manuscript

View Article Online
DOI: 10.1039/C7CP06709G

Published on 30 November 2017. Downloaded by University of Wisconsin - Madison on 30/11/2017 14:59:34.

consistent with the observation from multiple-ligand MM simulations that the amine ligand prefers a parallel orientation at the gold surface, presumably driven by favorable ligand/gold interactions. Compared to the case of a protonated amine, the PMF for the deprotonated case is shifted to shorter $d_{N,\text{surface}}$ values (e.g., the well is shifted from ∼4 Å to ∼3 Å); again, this likely reflects the larger desolvation penalty for a protonate ligand as it approaches the surface (also see discussions below in Sect.3.3).

In short, the PMF results for a single ligand at the diamond/water and gold/water interfaces further confirm that the amine ligand has distinct orientational preferences at the two surfaces. The preference to the parallel orientation at the gold surface reflects the stronger ligand/gold interactions, which in principle may have contributions from both electrostatic/induction (especially for a protonated amine[14]) and dispersion interactions. Since the gold/ligand interaction is described entirely with Lennard-Jones potentials in the INTERFACE force field used here, it is important to validate the MM results with QM and QM/MM simulations, which we turn to next.

3.2 QM and QM/MM Gas Phase Calculation

In this section, we conduct various QM(/MM) calculations for gas-phase systems to establish the proper QM level and QM region in subsequent QM/MM simulations in the condensed phase.

3.2.1 QM Cluster Models

To identify the proper QM level to use for QM/MM calculations, we first compare various DFT calculations to CCSD(T) results for the small cluster models shown in Fig. 2, which probe both covalent and non-covalent gold-ligand interactions, although the non-covalent interactions are of primary interest in this study. Since CCSD(T) is most reliable for systems whose electronic wavefunction is dominated by a single reference, we evaluate the T_1 diagnostics for all cases studied.[46,47] As summarized in Table S1 in **Supporting Information**,

Physical Chemistry Chemical Physics Accepted Manuscript

View Article Online
DOI: 10.1039/C7CP06709G

Published on 30 November 2017. Downloaded by University of Wisconsin - Madison on 30/11/2017 14:59:34.

Physical Chemistry Chemical Physics Accepted Manuscript

the values are generally not much higher than 0.02, especially for the non-covalent cases; for the covalent bonding situation described in Fig. 2a, the T_1 diagnostics approaches 0.03 for large Au-ligand distances, which might suggest less reliable predictions at the CCSD(T) levels for the dissociation curve at large d values in Fig. 7a. For the binding energies of interest, which are summarized in Table 1, the CCSD(T) results are expected to be reliable references. Another point worth noting is that the CCSD(T) results depend sensitively on the size and quality of the basis set; with the Hay-Wadt pseudo-potential and the corresponding basis set (Lanl2TZ[48]) for gold, as shown in Fig. S2 and Table S2 in **Supporting Information**, the energetics are substantially different, likely because the Hay-Wadt pseudo-potential and basis were not parameterized for correlated calculations.

Table 1: Vertical binding energy (E_{bd}, in kcal/mol) calculated with CCSD(T) and errors for various DFT functionals (in parentheses) for the systems shown in Fig. 2[a]

Method	(a)	(b)	(c)	(d)
CCSD(T)	-69.7	-87.8	-3.4	-20.4
PBE	(-2.5/2.2)	(1.9/-4.3)	(1.3/-0.2)	(1.9/4.9)
PBE-GD3	(-11.3/-7.4)	(-0.3/-6.6)	(-2.0/-3.9)	(-2.0/0.7)
B3LYP	(11.8/17.9)	(8.1/16.4)	(3.8/3.3)	(4.7/8.4)
B3LYP-GD3	(7.1/13.3)	(4.3/12.6)	(-1.8/-3.4)	(-1.9/0.8)
M06	(3.8/9.9)	(2.1/9.2)	(-0.1/-0.4)	(2.1/5.6)
M06-GD3	(3.3/9.4)	(1.5/8.6)	(-1.0/-1.2)	(1.3/4.7)
PBE0	(4.3/10.2)	(1.8/9.7)	(2.6/1.7)	(2.1/5.0)
PBE0-GD3	(1.5/7.4)	(-0.6/7.3)	(-0.9/-2.3)	(-1.8/0.5)
B2PLYP	(21.6/26.9)	(13.0/15.6)	(5.0/5.2)	(6.0/10.0)
B2PLYP-GD3	(18.9/24.2)	(10.7/13.3)	(1.8/1.4)	(2.3/5.7)
CAM-B3LYP	(8.8/1.9)	(0.2/-4.5)	(3.2/-0.2)	(3.1/4.9)
CAM-B3LYP-GD3	(5.6/-0.7)	(-2.5/-5.9)	(-0.7/-3.9)	(-1.4/0.7)
TPSSh	(4.6/9.7)	(2.5/9.5)	(3.1/1.5)	(2.7/5.2)

[a] Basis set for CCSD(T): cc-pVTZ-pp for Au, with the g functions removed, cc-pVTZ for the main group elements. Basis set for DFT: for values before the slash, the same basis set as CCSD(T) calculations; for values after the slash, Lanl2DZ for Au, 6-31G(d) for the main group elements.

From the potential energy scans shown in Fig. 7, which use the same basis set for CCSD(T) and DFT calculations, it is seen that B3LYP substantially underestimates both covalent and non-covalent interactions; PBE calculations, by contrast, trace the CCSD(T) results rather faithfully for all cases, with errors on the order of a few kcal/mol. The empiri-

View Article Online
DOI: 10.1039/C7CP06709G

Published on 30 November 2017. Downloaded by University of Wisconsin - Madison on 30/11/2017 14:59:34.

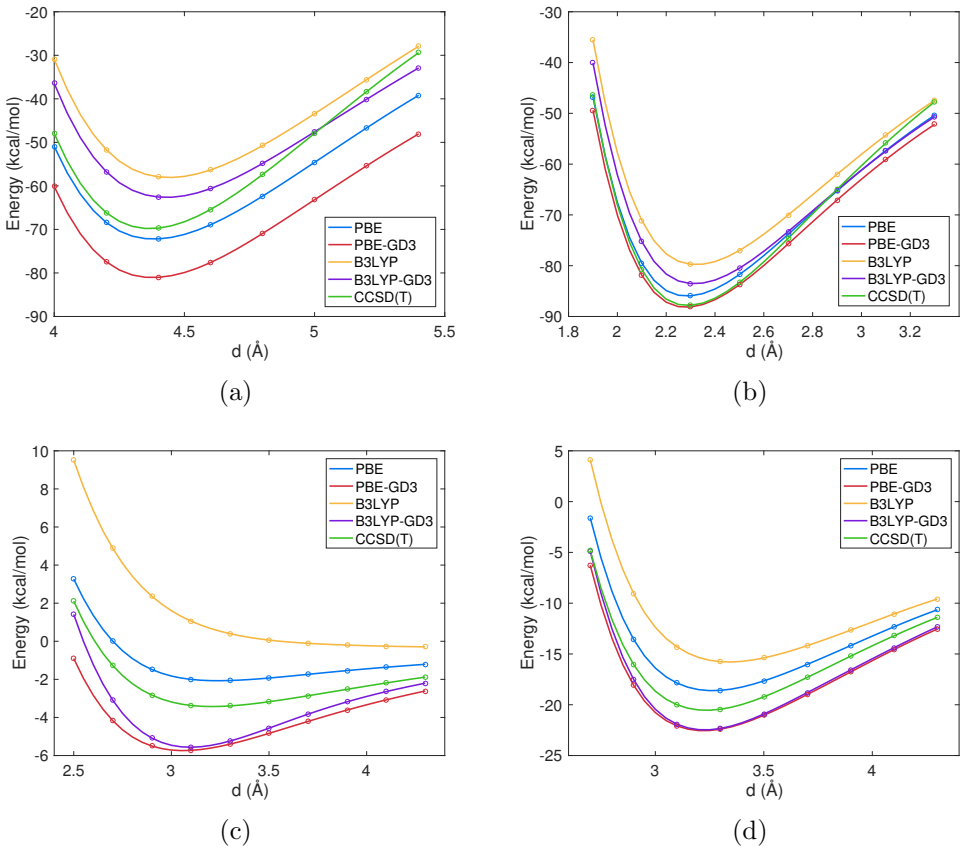

Figure 7: Potential energy scans using different methods for (a-b) covalent and (c-d) non-covalent interactions between the amine ligand and gold clusters shown in Figure 2. The variable for the horizontal axis, d, is indicated in Figure 2 with dash lines. Basis set: cc-pVTZ-pp for Au with the g functions removed, cc-pVTZ for the main group elements. Restricted and unrestricted references lead to identical results for all distances scanned here.

Physical Chemistry Chemical Physics Accepted Manuscript

View Article Online
DOI: 10.1039/C7CP06709G

Published on 30 November 2017. Downloaded by University of Wisconsin - Madison on 30/11/2017 14:59:34.

cal dispersion[27] contribution is relatively small, typically with a stabilization of 2-4 kcal/mol, although larger contribution is also observed in certain cases. Since non-covalent interactions are substantially weaker, the empirical dispersion correction makes a larger relative contribution in those cases. For the non-covalent interactions shown in Fig. 7c-d, PBE and PBE-GD3 results underestimate and overestimate the binding energy by a similar amount as compared to CCSD(T).

In Table 1, comparison is made with additional density functionals, including M06,[49] a double-hybrid functional (B2PLYP[50]), a range-separation functional (CAM-B3LYP[51]) and a meta-GGA functional (TPSSh[52,53]); some of them were found to be reliable for gold-ligand interactions in previous benchmark calculations for smaller systems.[28,29] Results here suggest that PBE and PBE-GD3 are the most reliable for the systems of interest here. Moreover, with these two functionals, using a substantially smaller basis set (Lanl2dz for Au and 6-31G(d) for main group elements) does not lead to much larger errors. Therefore, in the subsequent QM/MM calculations, which are computationally more demanding due to the need of sampling (for the condensed phase), we use the PBE-GD3 approach with the smaller basis set.

3.2.2 Gas phase QM/MM energy calculations

To identify the proper QM size in QM/MM simulations, gas phase QM/MM calculations for the single amine ligand at the (111) surface of a gold slab are conducted with different layers of gold atoms treated as QM (PBE-GD3); the quantity of interest is the relative energy of the optimized parallel and vertical ligand orientations.

As shown in Table 2, both QM and MM regions contribute to the additional stabilization of the parallel orientation over the vertical one, although the MM contribution (which is entirely van der Waals in nature since the MM gold atoms do not bear any partial charge in INTERFACE[11]) is relatively small and of a few kcal/mol; as expected, the MM contribution does not differ significantly with different amine protonation states, and the contribution

Physical Chemistry Chemical Physics Accepted Manuscript

View Article Online
DOI: 10.1039/C7CP06709G

Published on 30 November 2017. Downloaded by University of Wisconsin - Madison on 30/11/2017 14:59:34.

Table 2: Additional stabilization (in kcal/mol) of the parallel orientation over the vertical orientation with different QM regions (see Figure 3) in gas-phase QM/MM and periodic DFT calculations[a]

	ΔE_{QM}	ΔE_{MM}	ΔE_{tot}
QM/MM			
single-layer	34.7/9.5	6.6/4.3	41.3/13.8
double-layer	12.9/2.9	7.3/5.8	20.2/8.7
triple-layer	24.1/13.0	4.6/3.9	28.7/17.0
quadruple-layer	27.5/18.4	1.8/1.7	29.3/20.1
Periodic DFT[b]	—	—	47.7/41.6

[a] Numbers before and after the slash are for the protonated and deprotonated amine cases, respectively. [b] Computed using ligand orientations optimized by gas-phase QM/MM with the quadruple-layer QM model; the gold slab is fully optimized at the periodic DFT level. Thus the periodic DFT results gives an upper bound to the stability of the parallel orientation over the vertical one.

becomes rather small as the QM region extends to include four layers of gold atoms. The QM contribution, by contrast, is substantially larger in magnitude. The QM contribution for the protonated ligand is generally larger by ∼10 kcal/mol (except for the case of the single layer model) than the deprotonated ligand; this is to be expected considering the highly polarizable nature of gold. In terms of the QM size dependence, rather large differences are observed as the QM region gradually increases from the single-layer to the triple-layer. The difference between the triple-layer and quadruple-layer models, however, is more modest, especially for the total (QM/MM) stabilization energy. Considering the balance between accuracy and computational efficiency, we adopt the triple-layer QM region in the subsequent condensed phase QM/MM free energy simulations.

Table 3: Amount of charge transfer from the ligand to the gold slab according to Hirshfeld population analysis[a] for gas phase QM/MM and periodic DFT calculations.

Method	Deprotonated, vertical	Deprotonated, parallel	Protonated, vertical	Protonated, parallel
DFT/MM	-0.075	0.016	0.119	0.333
Periodic DFT	-0.088	0.057	0.275	0.563

[a] A full list of Hirschfeld charges is included in Table S3-S4 in **Supporting Information**.

Since bulk gold and most gold nanoparticles are metallic in nature, one question of interest is whether treating a relatively small (∼30) number of atoms as QM describes the electronic structure properly. To answer this question, we compare gas-phase DFT/MM and periodic

Physical Chemistry Chemical Physics Accepted Manuscript

View Article Online
DOI: 10.1039/C7CP06709G

Published on 30 November 2017. Downloaded by University of Wisconsin - Madison on 30/11/2017 14:59:34.

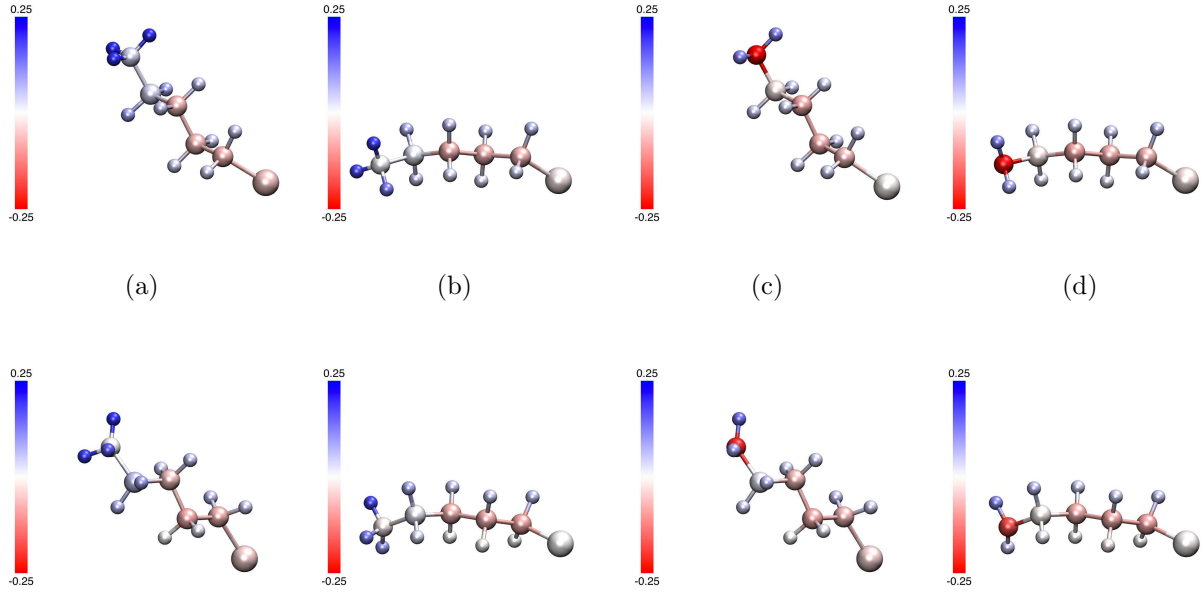

Figure 8: Hirschfeld charges for the ligand atoms in gas phase QM/MM (a-d) and periodic DFT (e-h) calculations for the (a-b,e-f) protonated and (c-d,g-h) deprotonated alkyl amine in different orientations. For clarity, the gold surface is not shown.

Physical Chemistry Chemical Physics Accepted Manuscript

View Article Online
DOI: 10.1039/C7CP06709G

Published on 30 November 2017. Downloaded by University of Wisconsin - Madison on 30/11/2017 14:59:34.

DFT results (see next subsection) for the relative stability of the two ligand orientations at the gold surface and also the corresponding charge distributions; in particular, a quantity of interest is the amount of charge transfer from the ligand to the gold slab, especially when the ligand adopts the parallel orientation. Results from the gas-phase QM/MM calculations are summarized in Fig. 8a-d and Table 3; to facilitate comparison with the periodic DFT calculations (see next subsection), we use the Hirshfeld population analysis[54–56] in both sets of calculations. As shown in Fig. 8a-d, partial charges on the ligand do not depend much on the orientation; in total, the amount of charge transferred to the QM region is very modest ($\leq$0.1), except for the protonated amine in the parallel orientation, for which the amount of charge transfer to the gold slab is $0.333e$.

3.2.3 Periodic DFT calculations

In the periodic DFT calculations, the preference to the parallel orientation is very strong; regardless of the initial orientation and amine protonation state, geometry optimization leads to the parallel orientation. Since it is less straightforward to conduct minimization in the presence of constraint in DMol^3, to estimate the stabilization of the parallel orientation over the vertical one, we take the ligand structure and its orientation relative to the gold surface from gas-phase QM/MM minimizations and compute periodic DFT energy calculations. As shown in Table 2, the calculations predict a significantly larger stabilization ($\sim$40 kcal/mol) to the parallel orientation. This is somewhat expected since the structure of the gold slab is taken from periodic DFT optimization with a parallel ligand, thus such calculation gives an upper bound to the stabilization of the parallel orientation. Similar to gas-phase QM/MM results, the stabilization is less for the deprotonated ligand by $\sim$6 kcal/mol.

The Hirschfeld charges on the ligands in different protonation states and orientations from the periodic DFT calculations are shown in Fig. 8e-h; they look generally similar to those from the gas-phase QM/MM calculations (Fig. 8a-d). Summing up the ligand charges leads to an estimate of the amount of charge transfer from the ligand to the gold

Physical Chemistry Chemical Physics Accepted Manuscript

View Article Online
DOI: 10.1039/C7CP06709G

Published on 30 November 2017. Downloaded by University of Wisconsin - Madison on 30/11/2017 14:59:34.

slab. As shown in Table 3, the amount of charge transfer in the periodic DFT calculations is generally larger in magnitude than the prediction of gas-phase QM/MM simulations; for example, for the protonated amine in the parallel orientation, the amount of charge transfer is $0.563e$ and $0.333e$ with periodic DFT and gas-phase QM/MM calculations, respectively. Nevertheless, the general trends (i.e., the amount of charge transfer as a function of ligand protonation state and orientation) are similar in the two types of calculations. Considering that solvation will further stabilize charges on the ligand and therefore reduce the amount of charge transfer to the gold slab, we conclude that the QM region in the current QM/MM calculations is expected to provide a realistic description for the charge distribution at the gold/water interface.

3.3 QM/MM Solution Simulations

The QM/MM-PMF minimizations lead to a local minimum for both the vertical and parallel orientations; we emphasize that due to the statistical errors in the QM/MM-PMF gradient,[41] a loose gradient threshold (RMS force $\leq$0.001667 hartree/bohr) is used in the geometry optimization. As shown in Table 4, The optimized $d_{N,\text{surface}}$ values are closer to those from gas-phase QM/MM minimizations than those from umbrella sampling using the MM model. In particular, while all three calculations predict a similar $d_{N,\text{surface}}$ ($\sim$3 Å) for the parallel orientation of the deprotonated ligand, only MM simulation finds that the optimal $d_{N,\text{surface}}$ value for the protonated ligand in the parallel orientation is shifted up by $\sim$1 Å; we note, however, that the MM PMF also features a shallow local minima around $d_{N,\text{surface}} \sim 3.5$ Å (Fig. 6b), which is $\sim$ 1 kcal/mol higher in free energy.

In terms of relative stability of the two ligand orientations, all three types of simulations lead to the same trend that the parallel orientation is strongly preferred (Table 4). The QM/MM-PMF and MM simulations find similar magnitudes of stabilization for the protonated ligand ($\sim 4-5$ kcal/mol); for the deprotonated ligand, MM simulation gives a weaker preference ($\sim$7 kcal/mol) than QM/MM-PMF calculations ($\sim$13 kcal/mol) to the parallel

Physical Chemistry Chemical Physics Accepted Manuscript

View Article Online
DOI: 10.1039/C7CP06709G

Published on 30 November 2017. Downloaded by University of Wisconsin - Madison on 30/11/2017 14:59:34.

Physical Chemistry Chemical Physics Accepted Manuscript

Table 4: Optimized vertical distance from amine nitrogen to the gold surface ($d_{N,\text{surface}}$, in Å) and stability (in kcal/mol) for the two ligand orientations in different simulations

	Deprotonated		Protonated	
	vertical	parallel	vertical	parallel
$d_{N,\text{surface}}$ (Å)				
Gas Phase QM/MM[a]	7.0	3.0	6.9	3.0
QM/MM-PMF	6.7	3.0	6.6	3.1
MM Umbrella Sampling	6.6	2.9	6.4	4.1/3.5[b]
Stability (kcal/mol)				
Gas Phase QM/MM[a]	17.0	0.0	28.7	0.0
QM/MM-PMF	12.6	0.0	5.0	0.0
MM Umbrella Sampling	6.9	0.0	3.8	0.0

[a] The results for gas phase QM/MM are based on the triple-layer QM model (see Table 2), which is also the QM region in the condensed phase QM/MM-PMF simulations. [b] The MM PMF features a shallow local minimum at ∼3.5 Å (see Fig. 6b).

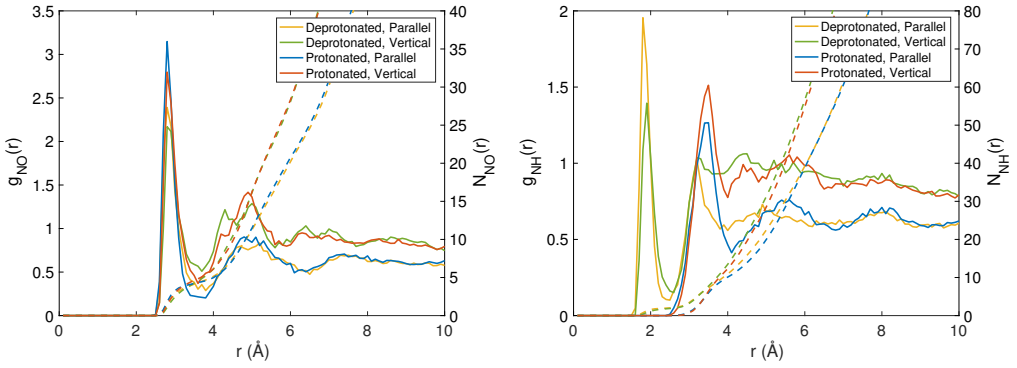

Figure 9: Radial distribution functions of the water oxygen and hydrogen around the amine nitrogen ($g_{NO}(r), g_{NH}(r)$) from the last iteration of QM/MM-PMF optimization, which contains 100 ps of sampling; the dashed lines indicate the integrated radial distribution functions, which give the number of water oxygen/hydrogen within a given distance from the amine nitrogen ($N_{NO}(r), N_{NH}(r)$). For comparison, results from MM simulations are shown in Fig. S3 in **Supporting Information**.

View Article Online
DOI: 10.1039/C7CP06709G

Published on 30 November 2017. Downloaded by University of Wisconsin - Madison on 30/11/2017 14:59:34.

orientation. The lower degree of stabilization for the protonated ligand in the parallel orientation likely reflects the higher degree of desolvation penalty as the protonated amine isomerizes from the vertical to the parallel orientation. This is illustrated by the radial distribution functions of water oxygen and hydrogen around the amine nitrogen (g_{NO}, g_{NH}) for the ligand in different protonation states and orientations (Fig. 9). Within ∼6 Å of the amine nitrogen, regardless of the protonation state, the vertical orientation features about eight more water than the parallel orientation; the impact of such difference on the amine solvation is expected to be larger in the protonated state due to its higher charge. Indeed, using a linear response model,[57] which estimates the relative solvation free energy of the two protonation states by computing the differential solute-solvent interaction energies, the protonated ligand has a higher solvation free energy than the deprotonated state by 112.6 and 106.0 kcal/mol in the vertical and parallel orientations, respectively. In other words, solvation is expected to decrease the stability of the parallel orientation by an additional ∼6 kcal/mol when the ligand is protonated; this is consistent with the results from both QM/MM-PMF and MM simulations shown in Table 4.

The effect of solvation is further highlighted by the comparison of gas-phase QM/MM and solution phase results. In contrast to the solution phase, the protonated ligand has a substantially larger preference (28.7 vs. 17.0 kcal/mol) to the parallel orientation. In the absence of solvation, the protonated ligand interacts much more favorably with the gold surface through electrostatic and induction effects than the deprotonated ligand. The dramatic reversal of the trend in solution simulations underscores the importance of including solvation effects for processes that occur at metal/water interface, especially when charged species are involved.

Overall, the agreement between MM and QM/MM-PMF simulations for the gold/water interface is not quantitative but encouraging. This is rather remarkable considering that the MM model used here (INTERFACE) treats the gold atoms as neutral and non-polarizable Lennard-Jones particles. This observation seems to suggest that the effective ligand-gold

Physical Chemistry Chemical Physics Accepted Manuscript

View Article Online
DOI: 10.1039/C7CP06709G

Published on 30 November 2017. Downloaded by University of Wisconsin - Madison on 30/11/2017 14:59:34.

interaction in the condensed phase is largely dictated by dispersion type of interactions, while electrostatic and induction effects, albeit being dominant in vacuum as reflected by the gas-phase results (e.g, the modest impact of empirical dispersion shown in Fig. 7 and significant dependence on the ligand protonation state shown in Table 2), are considerably quenched by the solvent.

3.4 Experimental Observables

Finally, we briefly discuss whether the different ligand orientations at the gold surface can be distinguished experimentally. Since the amine group features different environments in the parallel and vertical orientations, especially in terms of interactions with the gold surface and the level of solvation, we expect that spectroscopic techniques such as infrared[58] and Nuclear Magnetic Resonance (NMR)[59,60] are able to distinguish the two orientations. To motivate future experimental studies, we compute the NMR chemical shifts for the amine group when the ligand adopts different orientations at the gold surface; to ensure that all gold atoms close to the amine in the parallel orientation are treated at the QM level, a slightly larger QM region than the triple-layer QM/MM model is used for the NMR chemical shift calculations (see Fig. S5 in **Supporting Information**). As shown in Table 5, regardless of the protonation state, the closer proximity to the gold surface in the parallel orientation indeed leads to significant perturbations in the chemical shifts of the amine group and the carbon covalently bond to it. The nitrogen chemical shift is perturbed by more than 20 ppm, while those for the amine protons are also perturbed significantly, especially for the proton pointing toward the surface. For the carbon chemical shift, large difference (8-10 ppm) is observed between the two orientations for the protonated amine; by comparison, previous DFT calculations and ^{13}C solid state NMR studies[60] found an effect of 15-30 ppm for a carboxylate group when citrate binds to a gold nanoparticle. The basic trend and magnitude of perturbation remain largely similar with and without an implicit solvent model, suggesting that direct interaction with the nearby gold atoms dominates perturbations in

Physical Chemistry Chemical Physics Accepted Manuscript

View Article Online
DOI: 10.1039/C7CP06709G

Published on 30 November 2017. Downloaded by University of Wisconsin - Madison on 30/11/2017 14:59:34.

the chemical shifts. Therefore, we encourage future NMR studies to further characterize the binding modes of alkyl amines at the surface of gold nanoparticles in water.

Table 5: NMR chemical shifts (in ppm) for the amine group from cluster PBE calculations with and without an implicit solvent (PCM) contribution[a]

	Deprotonated		Protonated	
Gas phase	vertical	parallel	vertical	parallel
N	47.0	71.9	57.8	77.9
C	51.6	55.6	55.2	46.7
H	0.5	2.7	4.6	10.5
H	0.6	1.1	4.4	3.4
H	-	-	5.2	3.9
	Deprotonated		Protonated	
PCM[b]	vertical	parallel	vertical	parallel
N	41.7	72.9	56.4	74.2
C	51.0	52.5	53.3	45.4
H	0.7	6.2	4.8	9.2
H	0.8	3.1	4.7	3.7
H	-	-	5.3	3.3

[a] The Gauge-Independent Atomic Orbital (GIAO) method[61–65] is used to calculate the NMR chemical shifts for the amine group and the carbon covalently bound to it; for a snapshot of the cluster model used in the calculations, see Fig. S5 in **Supporting Information**. Basis set: Lanl2DZ[32] for Au and aug-cc-pVTZ[66,67] for the main group elements. The references are TMS/NH_3 (in the gas phase) for C,H/N. [b] The integral equation formalism variant of the polarizable continuum model (IEFPCM)[68–70] is applied with the UFF set of atomic radii.[71]

Physical Chemistry Chemical Physics Accepted Manuscript

View Article Online
DOI: 10.1039/C7CP06709G

Published on 30 November 2017. Downloaded by University of Wisconsin - Madison on 30/11/2017 14:59:34.

Physical Chemistry Chemical Physics Accepted Manuscript

4 Concluding Remarks

To understand the chemical properties of ligands at nanoparticle surfaces, such as their titration state, reactivity and binding with other molecules, it is crucial to determine the conformational properties of the ligands. While great progress is being made to integrate computations with multiple experimental approaches to determine the properties of surface ligands of nanoparticles,[59,60] most computations are limited to static DFT calculations, which do not sample the conformational heterogeneity of the ligands, nearby solvent and other species in solution (e.g., counter ions and other small solutes). Therefore, it is valuable to supplement DFT calculations with molecular dynamics (MD) simulations for a better characterization of nanoparticle/solution interfaces. Since MD simulations are most efficient with force field models, it is important to carefully calibrate force field models with QM based calculations and whenever possible, experimental data. The general challenge in this context is to establish calibration strategies that integrate QM calculations in the realistic condensed phase situations that force field models are developed for.

In this study, using a simple example of an alkyl amine ligand grafted to the surface of gold (111) surface, we illustrate the integration of multiple computational methods to analyze physical properties of solid/water interface; the findings are expected to apply to nanoparticle/water interface as well. The protocol involves using a correlated *ab initio* (CCSD(T)) method to first calibrate DFT as the QM approach, which is then used in QM/MM simulations to compute relevant free energy quantities at the gold/water interface; gas-phase QM/MM and periodic DFT calculations are used to determine the proper QM size in the QM/MM simulations. Finally, QM/MM free energy results are compared with those from MM simulations to explicitly calibrate the force field model for the gold/water interface; involving QM/MM calculations is crucial because it is generally not appropriate to compare empirical force field results with high-level QM calculations in the gas phase, and the key ingredient that makes the protocol feasible is the adaptation of the minimum free energy path approach of Yang and co-workers,[12] which decouples the sampling of the

View Article Online
DOI: 10.1039/C7CP06709G

Published on 30 November 2017. Downloaded by University of Wisconsin - Madison on 30/11/2017 14:59:34.

QM(DFT) atoms and MM atoms.

The specific free energy quantity of interest here is the relative stability of two ligand orientations at the gold/water interface, referred to as parallel and vertical orientations. While the vertical orientation is preferred at the diamond/water interface, MM simulations suggest that the parallel orientation is favored at the gold/water interface, even at a moderate ligand density close to that for functionalized gold nanoparticles prepared in recent experimental studies; such a difference is expected to impact the pK_a and thus charge properties of the ligands and, in turn, the interaction between the gold nanoparticle with other (bio)molecules in solution. We have shown through NMR chemical shift calculations that the two orientations in principle can be distinguished based on N/C/H chemical shifts; we hope our calculations motivate future experimental studies, along the lines of Refs. 59,60.

Our calculations find that the widely used PBE functional in materials studies is one of the most reliable functionals for the gold-ligand interaction of interest; the impact of empirical dispersion (GD3) is found to be modest, presumably because the ligand is relatively small in size. PBE-GD3/MM simulations generally support the finding of the MM simulations, in terms of the geometry and stability of the two orientations for both protonation states of the amine ligand. The general agreement is encouraging since the the INTERFACE model used here treats the gold atoms as non-polarizable Lennard-Jones particles. Thus the results support the use of a van der Waals model to effectively describe gold/ligand interactions in the condensed phase as contributions from electrostatic and induction are significantly quenched by solvation. Indeed, while the parallel orientation is much favored by the protonated amine in gas phase QM/MM and periodic DFT calculations, it is the deprotonated ligand that exhibits a higher degree of preference toward the parallel orientation in solution; although the MM model does not capture the dramatic difference between the two protonation states in the gas-phase, the solution phase results are consistent with the QM/MM simulations. These observations highlight the importance of treating solvation for charged systems at the metal/water interface, and the need of using condensed phase

Physical Chemistry Chemical Physics Accepted Manuscript

View Article Online
DOI: 10.1039/C7CP06709G

Published on 30 November 2017. Downloaded by University of Wisconsin - Madison on 30/11/2017 14:59:34.

simulations to calibrate empirical force field models.

At the quantitative level, the discrepancy between the MM and QM/MM results (Table 4) suggests potential improvement of the force field model, such as explicitly including electronic polarization, which has been incorporated in a recent gold force field[72] and also being developed for INTERFACE (Heinz, private communication). Both QM/MM and periodic DFT calculations in the gas phase reveal a non-trivial amount of charge transfer from the ligand to the gold slab (with a Hirschfeld population scheme), similar to observations from recent DFT analysis of citrate-gold surface interactions.[60] Since solvation is expected to stabilize ligand charge, whether it is essential to explicitly treat charge transfer effects in force fields[73] for gold remains to be analyzed systematically in the future. In addition, while QM/MM calculations with about 30 gold atoms treated at the QM level qualitatively agree with periodic DFT calculations in the gas-phase, there are also quantitative differences in terms of energetics and charge distributions (see Tables 2 and 3). Future efforts to better couple QM with polarizable MM[74–76] will further improve the quantitative accuracy of QM/MM simulations for materials/solution interfaces.

Finally, we note that the technical issues discussed here are not limited to nanoparticle/solution interfaces, but relevant to many other problems that involve both inorganic/metallic and organic/biomolecular components, such as heterogeneous catalysis,[77] biomineralization[78] and electrochemistry.[79] Therefore, we expect that our strategy of integrating multiple computational approaches to cross-validate each other is applicable to a broad range of complex interfacial systems.

Acknowledgement

This work was supported by NSF under the Center for Sustainable Nanotechnology, CHE-1503408. Computational resources from the Extreme Science and Engineering Discovery Environment (XSEDE), which is supported by NSF grant number OCI-1053575, are greatly

Physical Chemistry Chemical Physics Accepted Manuscript

View Article Online
DOI: 10.1039/C7CP06709G

appreciated; computations are also supported in part by NSF through a major instrumentation grant (CHE-0840494) to the Chemistry department.

Published on 30 November 2017. Downloaded by University of Wisconsin - Madison on 30/11/2017 14:59:34.

Physical Chemistry Chemical Physics Accepted Manuscript

Supporting Information

Additional benchmark calculations, Hirshfeld charges from gas-phase QM/MM and periodic DFT calculations, and discussion of ESP charge scheme in solution phase QM/MM-PMF simulations.

References

(1) Murphy, C. J.; Vartanian, A. M.; Geiger, F. M.; Hamers, R. J.; Pedersen, J.; Cui, Q.; Haynes, C. L.; Carlson, E. E.; Hernandez, R.; Klaper, R. D.; Orr, G.; Rosenzweig, Z. Biological responses to engineered nanomaterials: Needs for the next decade. *ACS Cent. Sci.* **2015**, *1*, 117.

(2) Cui, Q.; Hernandez, R.; Mason, S. E.; Frauenheim, T.; Pedersen, J. A.; Geiger, F. Sustainable nanotechnology: opportunities and challenges for theoretical/computational studies. *J. Phys. Chem. B* **2016**, *120*, 7297–7306.

(3) Troiano, J. M.; Olenick, L. L.; Kuech, T. R.; Melby, E. S.; Hu, D. H.; Lohse, S. E.; Mensch, A. C.; Dogangun, M.; Vartanian, A. M.; M. D. Torelli et al., Direct Probes of 4-nm Diameter Gold Nanoparticles Interacting with Supported Lipid Bilayers. *J. Phys. Chem. C* **2015**, *119*, 534–546.

(4) Dominguez, G. A.; Lohse, S. E.; Torelli, M. D.; Murphy, C. J.; Hamers, R. J.; Orr, G.; Klaper, R. D. Effects of charge and surface ligand properties of nanoparticles on oxidative stress and gene expression within the gut of Daphnia magna. *Aquat. Toxicol.* **2015**, *162*, 1 – 9.

View Article Online
DOI: 10.1039/C7CP06709G

Published on 30 November 2017. Downloaded by University of Wisconsin - Madison on 30/11/2017 14:59:34.

(5) Koivisto, J.; Chen, X.; Donnini, S.; Lahtinen, T.; Häkkinen, H.; Groenhof, G.; Pettersson, M. AcidBase Properties and Surface Charge Distribution of the Water- Soluble $Au_{102}(pMBA)_{44}$ Nanocluster. *J. Phys. Chem. C* **2016**, *120*, 10041–10050.

(6) Hong, J.; Hamers, R. J.; Pedersen, J. A.; Cui, Q. A Hybrid Molecular Dynamics/Multiconformer Continuum Electrostatics (MD/MCCE) Approach for the Determination of Surface Charge of Nanomaterials. *J. Phys. Chem. C* **2017**, *121*, 3584–3596.

(7) Altabet, Y. E.; Haji-Akbari, A.; Debenedetti, P. G. Effect of material flexibility on the thermodynamics and kinetics of hydrophobically induced evaporation of water. *Proc. Natl. Acad. Sci. USA* **2017**, *114*, E2548–E2555.

(8) MacKerell, A. D.; Bashford, D.; Bellott, M.; Dunbrack, R. L.; Evanseck, J. D.; Field, M. J.; Fischer, S.; Gao, J.; Guo, H.; S. Ha et al., All-Atom Empirical Potential for Molecular Modeling and Dynamics Studies of Proteins. *J. Phys. Chem. B* **1998**, *102*, 3586–3616.

(9) Huang, J.; A. D. MacKerell Jr., CHARMM36 All-atom Additive Protein Force Field: Validation Based on Comparison to NMR Data. *J. Comput. Chem.* **2013**, *34*, 2135–2145.

(10) Cornell, W. D.; Cieplak, P.; Bayly, C. I.; Gould, I. R.; Merz, K. M.; Ferguson, D. M.; Spellmeyer, D. C.; Fox, T.; Caldwell, J. W.; Kollman, P. A. A second generation force field for the simulation of proteins, nucleic acids, and organic molecules. *J. Am. Chem. Soc.* **1995**, *117*, 5179–5197.

(11) Heinz, H.; Lin, T.-J.; Mishra, R. K.; Emami, F. S. Thermodynamically Consistent Force Fields for the Assembly of Inorganic, Organic, and Biological Nanostructures: The INTERFACE Force Field. *Langmuir* **2013**, *29*, 1754–1765.

(12) Hu, H.; Lu, Z.; Parks, J. M.; Burger, S. K.; Yang, W. Quantum mechanics/molecular mechanics minimum free-energy path for accurate reaction energetics in solution and

Physical Chemistry Chemical Physics Accepted Manuscript

View Article Online
DOI: 10.1039/C7CP06709G

Published on 30 November 2017. Downloaded by University of Wisconsin - Madison on 30/11/2017 14:59:34.

enzymes: Sequential sampling and optimization on the potential of mean force surface. *J. Chem. Phys.* **2008**, *128*, 034105.

(13) Heinz, H.; Ramezani-Dakhel, H. Simulations of inorganic–bioorganic interfaces to discover new materials: insights, comparisons to experiment, challenges, and opportunities. *Chem. Soc. Rev.* **2016**, *45*, 412–448.

(14) Heinz, H.; Jha, K. C.; Luettmer-Strathmann, J.; Farmer, B. L.; Naik, R. R. Polarization at metal–biomolecular interfaces in solution. *J. R. Soc. Interface* **2011**, *8*, 220–232.

(15) Jorgensen, W. L.; Chandrasekhar, J.; Madura, J. D.; Impey, R. W.; Klein, M. L. Comparison of simple potential functions for simulating liquid water. *J. Chem. Phys.* **1983**, *79*, 926–935.

(16) Torelli, M. D.; Putans, B. A.; Tan, Y. Z.; Lohse, S. E.; Murphy, C. J.; Hamers, R. J. Quantitative Determination of Ligand Densities on Nanomaterials by X-Ray Photoelectron Spectroscopy. *ACS Appl. Mater. & Inter.* **2015**, *7*, 1720–1725.

(17) Darden, T.; York, D.; Pedersen, L. Particle mesh Ewald: An Nlog (N) method for Ewald sums in large systems. *J Chem Phys* **1993**, *98*, 10089–10092.

(18) Steinbach, P. J.; Brooks, B. R. New spherical-cutoff methods for long-range forces in macromolecular simulation. *J. Comput. Chem.* **1994**, *15*, 667–683.

(19) Andersen, H. C. Rattle: A "Velocity" Version of the Shake Algorithm for Molecular Dynamics Calculations. *J. Comp. Phys.* **1983**, *52*, 24–34.

(20) Kumar, S.; Bouzida, D.; Swendsen, R. H.; Kollman, P. A.; Rosenberg, J. M. The weighted histogram analysis method for free-energy calculations on biomolecules I. The method. *J. Comput. Chem.* **1992**, *13*, 1011–1021.

(21) Perdew, J. P.; Burke, K.; Ernzerhof, M. Generalized gradient approximation made simple. *Phys. Rev. Lett.* **1996**, *77*, 3865.

Physical Chemistry Chemical Physics Accepted Manuscript

View Article Online
DOI: 10.1039/C7CP06709G

Published on 30 November 2017. Downloaded by University of Wisconsin - Madison on 30/11/2017 14:59:34.

(22) Perdew, J. P.; Burke, K.; Ernzerhof, M. Generalized Gradient Approximation Made Simple [Phys. Rev. Lett. 77, 3865 (1996)]. *Phys. Rev. Lett.* **1997**, *78*, 1396–1396.

(23) Becke, A. D. Density-functional thermochemistry. III. The role of exact exchange. *J. Chem. Phys.* **1993**, *98*, 5648–5652.

(24) Lee, C.; Yang, W.; Parr, R. G. Development of the Colle-Salvetti correlation-energy formula into a functional of the electron density. *Phys. Rev. B* **1988**, *37*, 785.

(25) Vosko, S. H.; Wilk, L.; Nusair, M. Accurate spin-dependent electron liquid correlation energies for local spin density calculations: a critical analysis. *Can. J. Phys.* **1980**, *58*, 1200–1211.

(26) Stephens, P.; Devlin, F.; Chabalowski, C.; Frisch, M. J. Ab initio calculation of vibrational absorption and circular dichroism spectra using density functional force fields. *J. Phys. Chem.* **1994**, *98*, 11623–11627.

(27) Grimme, S.; Antony, J.; Ehrlich, S.; Krieg, H. A consistent and accurate ab initio parametrization of density functional dispersion correction (DFT-D) for the 94 elements H-Pu. *J. Chem. Phys.* **2010**, *132*, 154104.

(28) Rajský, T.; Urban, M. Au_n (n= 1, 11) Clusters Interacting With Lone-Pair Ligands. *J Phys. Chem. A* **2016**, *120*, 3938–3949.

(29) Kepp, K. P. Benchmarking Density Functionals for Chemical Bonds of Gold. *J. Phys. Chem. A* **2017**, *121*, 2022–2034.

(30) Dunning Jr, T. H. Gaussian basis sets for use in correlated molecular calculations. I. The atoms boron through neon and hydrogen. *J. Chem. Phys.* **1989**, *90*, 1007–1023.

(31) Peterson, K. A.; Puzzarini, C. Systematically convergent basis sets for transition metals. II. Pseudopotential-based correlation consistent basis sets for the group 11 (Cu, Ag, Au) and 12 (Zn, Cd, Hg) elements. *Theor. Chem. Acc.* **2005**, *114*, 283–296.

Physical Chemistry Chemical Physics Accepted Manuscript

View Article Online
DOI: 10.1039/C7CP06709G

Published on 30 November 2017. Downloaded by University of Wisconsin - Madison on 30/11/2017 14:59:34.

(32) Hay, P. J.; Wadt, W. R. Ab initio effective core potentials for molecular calculations. Potentials for K to Au including the outermost core orbitals. *J. Chem. Phys.* **1985**, *82*, 299–310.

(33) Petersson, a.; Bennett, A.; Tensfeldt, T. G.; Al-Laham, M. A.; Shirley, W. A.; Mantzaris, J. A complete basis set model chemistry. I. The total energies of closed-shell atoms and hydrides of the first-row elements. *J. Chem. Phys.* **1988**, *89*, 2193–2218.

(34) Petersson, G.; Al-Laham, M. A. A complete basis set model chemistry. II. Open-shell systems and the total energies of the first-row atoms. *J. Chem. Phys.* **1991**, *94*, 6081–6090.

(35) Frisch, M. J.; Trucks, G. W.; Schlegel, H. B.; Scuseria, G. E.; Robb, M. A.; Cheeseman, J. R.; Scalmani, G.; Barone, V.; Mennucci, B.; Petersson, G. A.; Nakatsuji, H.; Caricato, M.; Li, X.; Hratchian, H. P.; Izmaylov, A. F.; Bloino, J.; Zheng, G.; Sonnenberg, J. L.; Hada, M.; Ehara, M.; Toyota, K.; Fukuda, R.; Hasegawa, J.; Ishida, M.; Nakajima, T.; Honda, Y.; Kitao, O.; Nakai, H.; Vreven, T.; Montgomery, J. A., Jr.; Peralta, J. E.; Ogliaro, F.; Bearpark, M.; Heyd, J. J.; Brothers, E.; Kudin, K. N.; Staroverov, V. N.; Kobayashi, R.; Normand, J.; Raghavachari, K.; Rendell, A.; Burant, J. C.; Iyengar, S. S.; Tomasi, J.; Cossi, M.; Rega, N.; Millam, J. M.; Klene, M.; Knox, J. E.; Cross, J. B.; Bakken, V.; Adamo, C.; Jaramillo, J.; Gomperts, R.; Stratmann, R. E.; Yazyev, O.; Austin, A. J.; Cammi, R.; Pomelli, C.; Ochterski, J. W.; Martin, R. L.; Morokuma, K.; Zakrzewski, V. G.; Voth, G. A.; Salvador, P.; Dannenberg, J. J.; Dapprich, S.; Daniels, A. D.; Farkas, Ö.; Foresman, J. B.; Ortiz, J. V.; Cioslowski, J.; Fox, D. J. Gaussian09 Revision D.01. Gaussian Inc. Wallingford CT 2009.

(36) Delley, B. An All-Electron Numerical Method for Solving the Local Density Functional for Polyatomic Molecules. *J. Chem. Phys.* **1990**, *92*, 508–517.

Physical Chemistry Chemical Physics Accepted Manuscript

View Article Online
DOI: 10.1039/C7CP06709G

Published on 30 November 2017. Downloaded by University of Wisconsin - Madison on 30/11/2017 14:59:34.

(37) Delley, B. From Molecules to Solids with the DMol^3 Approach. *J. Chem. Phys.* **2000**, *113*, 7556–7564.

(38) Monkhorst, H. J.; Pack, J. D. Special Points for Brillouin-Zone Integrations. *Phys. Rev. B* **1976**, *13*, 5188–5192.

(39) Singh, U. C.; Kollman, P. A. An approach to computing electrostatic charges for molecules. *J. Comput. Chem.* **1984**, *5*, 129–145.

(40) Besler, B. H.; Merz, K. M.; Kollman, P. A. Atomic charges derived from semiempirical methods. *J. Comput. Chem.* **1990**, *11*, 431–439.

(41) Lu, X.; Fang, D.; Ito, S.; Okamoto, Y.; Ovchinnikov, V.; Cui, Q. QM/MM Free Energy Simulations: Recent Progress and Challenges. *Mol. Simul.* **2016**, *42*, 1056–1078.

(42) Brooks, B. R.; III, C. L. B.; Mackerell, A. D.; Nilsson, L.; Petrella, R. J.; Roux, B.; Won, Y.; Archontis, G.; Bartels, C.; Boresch, S.; Caflisch, A.; Caves, L.; Cui, Q.; Dinner, A. R.; Feig, M.; Fischer, S.; Gao, J.; Hodoscek, M.; Im, W.; Kuczera, K.; Lazaridis, T.; Ma, J.; Ovchinnikov, V.; Paci, E.; Pastor, R. W.; Post, C. B.; Pu, J. Z.; Schaefer, M.; Tidor, B.; Venable, R. M.; Woodcock, H. L.; Wu, X.; Yang, W.; York, D. M.; Karplus, M. CHARMM: The Biomolecular Simulation Program. *J. Comput. Chem.* **2009**, *30*, 1545–1614.

(43) C. L. Brooks III,; Karplus, M. Deformable stochastic boundaries in molecular dynamics. *J. Chem. Phys.* **1983**, *79*, 6312–6325.

(44) McQuarrie, D. A. *Statistical Mechanics*; Harper and Row, 1973.

(45) Lee, J.; Im, W. Transmembrane helix tilting: Insights from calculating the potential of mean force. *Phys. Rev. Lett.* **2008**, *100*, 018103.

(46) Lee, T. J.; Taylor, P. R. A diagnostic for determining the quality of single-reference electron correlation methods. *Int. J. Quantum Chem.* **1989**, *36*, 199–207.

Physical Chemistry Chemical Physics Accepted Manuscript

View Article Online
DOI: 10.1039/C7CP06709G

Published on 30 November 2017. Downloaded by University of Wisconsin - Madison on 30/11/2017 14:59:34.

(47) Jiang, W.; DeYonker, N. J.; Wilson, A. K. Multireference character for 3d transition-metal-containing molecules. *J. Chem. Theory Comput.* **2012**, *8*, 460–468.

(48) Roy, L. E.; Hay, P. J.; Martin, R. L. Revised basis sets for the LANL effective core potentials. *J. Chem. Theory Comput.* **2008**, *4*, 1029–1031.

(49) Zhao, Y.; Schultz, N. E.; Truhlar, D. Exchange-correlation functional with broad accuracy for metallic and nonmetallic compounds, kinetics, and noncovalent interactions. *J. Chem. Phys.* **2005**, *123*, 161103.

(50) Goerigk, L.; Grimme, S. Efficient and Accurate Double-Hybrid-Meta-GGA Density Functionals Evaluation with the Extended GMTKN30 Database for General Main Group Thermochemistry, Kinetics, and Noncovalent Interactions. *J. Chem. Theory Comput.* **2010**, *7*, 291–309.

(51) Yanai, T.; Tew, D. P.; Handy, N. C. A new hybrid exchange–correlation functional using the Coulomb-attenuating method (CAM-B3LYP). *Chem. Phys. Lett.* **2004**, *393*, 51–57.

(52) Tao, J.; Perdew, J. P.; Staroverov, V. N.; Scuseria, G. E. Climbing the density functional ladder: Nonempirical meta–generalized gradient approximation designed for molecules and solids. *Phys. Rev. Lett.* **2003**, *91*, 146401.

(53) Staroverov, V. N.; Scuseria, G. E.; Tao, J.; Perdew, J. P. Comparative assessment of a new nonempirical density functional: Molecules and hydrogen-bonded complexes. *J. Chem. Phys.* **2003**, *119*, 12129–12137.

(54) Hirshfeld, F. L. Bonded-atom fragments for describing molecular charge densities. *Theor. Chem. Acc.* **1977**, *44*, 129–138.

(55) Ritchie, J. P. Electron density distribution analysis for nitromethane, nitromethide, and nitramide. *J. Am. Chem. Soc.* **1985**, *107*, 1829–1837.

Physical Chemistry Chemical Physics Accepted Manuscript

View Article Online
DOI: 10.1039/C7CP06709G

Published on 30 November 2017. Downloaded by University of Wisconsin - Madison on 30/11/2017 14:59:34.

(56) Ritchie, J. P.; Bachrach, S. M. Some methods and applications of electron density distribution analysis. *J. Comput. Chem.* **1987**, *8*, 499–509.

(57) Warshel, A. *Computer Modeling of Chemical Reactions in Enzymes and Solution*; Wiley, New York, 1991.

(58) Park, J. W.; Shumaker-Parry, J. S. Structural Study of Citrate Layers on Gold Nanoparticles: Role of Intermolecular Interactions in Stabilizing Nanoparticles. *J. Am. Chem. Soc.* **2014**, *136*, 1907–1921.

(59) Salorinne, K.; Malola, S.; Wong, O. A.; Rithner, C. D.; Chen, X.; Ackerson, C. J.; Häkkinen, H. Conformation and dynamics of the ligand shell of a water-soluble Au_{102} nanoparticle. *Nat. Comm.* **2015**, *7*, 10401.

(60) Al-Johani, H.; Abou-Hamad, E.; Jedidi, A.; Widdifield, C. M.; Viger-Gravel, J.; Sangaru, S. S.; Gajan, D.; Anjum, D. H.; Ould-Chikh, S.; Hedhili, M. N.; Gurinov, A.; Kelly, M. J.; M. El Eter,; Cavallo, L.; Emsley, L.; Basset, J.-M. The structure and binding mode of citrate in the stabilization of gold nanoparticles. *Nat. Chem.* **2017**, *9*, 890–895.

(61) London, F. Théorie quantique des courants interatomiques dans les combinaisons aromatiques. *J. Phys. Radium* **1937**, *8*, 397–409.

(62) McWeeny, R. Perturbation theory for the Fock-Dirac density matrix. *Phys. Rev.* **1962**, *126*, 1028.

(63) Ditchfield, R. Self-consistent perturbation theory of diamagnetism: I. A gauge-invariant LCAO method for NMR chemical shifts. *Mol. Phys.* **1974**, *27*, 789–807.

(64) Wolinski, K.; Hinton, J. F.; Pulay, P. Efficient implementation of the gauge-independent atomic orbital method for NMR chemical shift calculations. *J. Am. Chem. Soc.* **1990**, *112*, 8251–8260.

Physical Chemistry Chemical Physics Accepted Manuscript

View Article Online
DOI: 10.1039/C7CP06709G

Published on 30 November 2017. Downloaded by University of Wisconsin - Madison on 30/11/2017 14:59:34.

(65) Cheeseman, J. R.; Trucks, G. W.; Keith, T. A.; Frisch, M. J. A comparison of models for calculating nuclear magnetic resonance shielding tensors. *J. Chem. Phys.* **1996**, *104*, 5497–5509.

(66) Kendall, R. A.; Dunning Jr, T. H.; Harrison, R. J. Electron affinities of the first-row atoms revisited. Systematic basis sets and wave functions. *J. Chem. Phys.* **1992**, *96*, 6796–6806.

(67) Woon, D. E.; Dunning Jr, T. H. Gaussian basis sets for use in correlated molecular calculations. III. The atoms aluminum through argon. *J. Chem. Phys.* **1993**, *98*, 1358–1371.

(68) Miertuš, S.; Scrocco, E.; Tomasi, J. Electrostatic interaction of a solute with a continuum. A direct utilizaion of AB initio molecular potentials for the prevision of solvent effects. *Chem. Phys.* **1981**, *55*, 117–129.

(69) Miertus, S.; Tomasi, J. Approximate evaluations of the electrostatic free energy and internal energy changes in solution processes. *Chem. Phys.* **1982**, *65*, 239–245.

(70) Pascual-ahuir, J.-L.; Silla, E.; Tunon, I. GEPOL: An improved description of molecular surfaces. III. A new algorithm for the computation of a solvent-excluding surface. *J. Comput. Chem.* **1994**, *15*, 1127–1138.

(71) Rappé, A. K.; Casewit, C. J.; Colwell, K.; Goddard Iii, W.; Skiff, W. UFF, a full periodic table force field for molecular mechanics and molecular dynamics simulations. *J. Am. Chem. Soc.* **1992**, *114*, 10024–10035.

(72) Wright, L. B.; Rodger, P. M.; Corni, S.; Walsh, T. R. GoIP-CHARMM: First-Principles Based Force Fields for the Interaction of Proteins with Au(111) and Au(100). *J. Chem. Theory Comput.* **2013**, *9*, 1616–1630.

Physical Chemistry Chemical Physics Accepted Manuscript

View Article Online
DOI: 10.1039/C7CP06709G

Published on 30 November 2017. Downloaded by University of Wisconsin - Madison on 30/11/2017 14:59:34.

(73) Yao, Y.; Kanai, Y.; Berkowitz, M. L. Role of Charge Transfer in Water Diffusivity in Aqueous Ionic Solutions. *J. Phys. Chem. Lett.* **2014**, *5*, 2711–2716.

(74) Sokol, A. A.; Bromley, S. T.; French, S. A.; Richard, C.; Catlow, A.; Sherwood, P. Hybrid QM/MM Embedding Approach for the Treatment of Localized Surface States in Ionic Materials. *Int. J. Quant. Chem.* **2004**, *99*, 695–712.

(75) Metz, S.; Kästner, J.; Sokol, A. A.; Keal, T. W.; Sherwood, P. ChemShell - a Modular Software Package for QM/MM Simulations. *WIREs Comput. Mol. Sci.* **2014**, *4*, 101–110.

(76) Huang, J.; Mei, Y.; König, G.; Simmonett, A. C.; Pickard IV, F. C.; Wu, Q.; Wang, L.-P.; MacKerell Jr, A. D.; Brooks, B. R.; Shao, Y. An Estimation of Hybrid Quantum Mechanical Molecular Mechanical (QM/MM) Polarization Energies for Small Molecules Using Polarizable Force-Field Approaches. *J. Chem. Theory Comput.* **2017**, *13*, 679.

(77) R. A. van Santen,; Neurock, M.; Shetty, S. G. Reactivity Theory of Transition-Metal Surfaces: A Bronsted-Evans-Polanyi Linear Activation Energy-Free-Energy Analysis. *Chem. Rev.* **2010**, *110*, 2005–2048.

(78) Walsh, T. R. Pathways to Structure-Property Relationships of Peptide-Materials Interfaces: Challenges in Predicting Molecular Structures. *Acc. Chem. Res.* **2017**, *7*, 1617–1624.

(79) Kattirtzi, J. A.; Limmer, D. T.; Willard, A. P. Microscopic dynamics of charge separation at the aqueous electrochemical interface. *Proc. Natl. Acad. Sci. USA* **2017**, *In press*.

Physical Chemistry Chemical Physics Accepted Manuscript

View Article Online
DOI: 10.1039/C7CP06709G

TOC Graphics

Published on 30 November 2017. Downloaded by University of Wisconsin - Madison on 30/11/2017 14:59:34.

Physical Chemistry Chemical Physics Accepted Manuscript